Enhanced Resonator Sensitivity with Nanostructured Porous Silica Coatings

S. H. Bhansali, J. M. Jarvis, I. A. Aksay,* and J. D. Carbeck

Department of Chemical Engineering, Princeton University, Princeton, New Jersey 08544-5263

We present a strategy to increase the sensitivity of resonators to the presence of specific molecules in the gas phase, measured by the change in resonant frequency as the partial pressure of the molecule changes. We used quartz crystals as the resonators and coated them with three different thin films (<1 μm thick) of porous silica: silica xerogel, silica templated by an ordered hexagonal phase of surfactant micelles, and silica templated by an isotropic L_3 phase surfactant micellar system. We compared the sensitivity of coated resonators to the presence of water vapor. The crystals coated with hexagonal phase-templated silica displayed a sensitivity enhancement up to 100-fold compared to an uncoated quartz crystal in the low-pressure regime where adsorption played a dominant role. L_3 phase-templated silica displayed the highest sensitivity (up to a 4000-fold increase) in the high partial pressure regimes where capillary condensation was the main accumulation mechanism. Three parameters differentiate the contributions of these coatings to the sensitivity of the underlying resonator: (i) specific surface area per unit mass of the coating, (ii) accessibility of the surfaces to a target molecule, and (iii) distribution in the characteristic radii of curvature of internal surfaces, as measured by capillary condensation.

Introduction

The resonant frequency of a mechanical oscillator, or resonator, is a function of the mass of the oscillating body. Resonators can be constructed to detect the accumulation of molecules or atoms; examples include quartz crystal microbalances (QCMs), silicon microcantilevers, and surface acoustic wave (SAW) devices.[1–4] Such resonators have been used to detect conversion in biocatalytic reactions,[1,2] molecular recognition events,[3] and the presence of volatile organic compounds, such as nerve gas agents used in chemical warfare.[4] The objective of this work is to describe a strategy for increasing the sensitivity of a resonator to the presence of a specific molecule in the gas phase (in this case, water vapor), as measured by a change in resonant frequency in response to a change in the partial pressure of the molecule. We do this by coating the surface of a resonator (in this case, a QCM) with thin films of nanostructured porous silica.

Sensitivity Improvement. For a given resonator, the intrinsic sensitivity is typically defined as the change in resonant frequency, f, per unit increase in the mass, m_i, due to the adsorption of the specific molecule, df/dm_i.[5–9] We propose a measure of sensitivity that is more appropriate to the application of resonators as sensors: the change in resonant frequency in response to a change in concentration of the species to be detected. If the species are in the gas phase, then the sensitivity of the sensor is defined as the change in resonant frequency per unit increase in partial pressure, P_i of the target species, df/dP_i. We relate these two definitions of sensitivity as

$$\frac{df}{dP_i} = f\left[\left(\frac{df}{dm_i}\right)\left(\frac{dm_i}{dP_i}\right)\right] \quad (1)$$

One approach to increasing the overall sensitivity is to increase the intrinsic sensitivity of the resonator, df/dm_i by altering its geometric, mechanical, or piezoelectric properties.[7,8] A second approach is to increase the mass of molecules that accumulate per unit increase in partial pressure, dm_i/dP_i, as we demonstrate in this work with nanostructured porous thin films.

Mass accumulation as a function of the partial pressure of accumulating species is typically referred to as "adsorption isotherms" or "BET isotherms", a practice that dates back to the work of Brunauer, Emmett, and Teller.[10] In addition to adsorption, the condensation of liquid in pores or channels can play a significant role in mass accumulation.[11,12] Thus, the terms "adsorption isotherm" and "BET isotherm" are both misnomers when the accumulation of mass involves phenomena other than just adsorption.

The simplest model of adsorption is the monolayer model of Langmuir.[13] In this model, the energetics of interaction between adsorbing molecules and sites on the surface is described by a constant, K, and the average number of bound molecules, n, per number of sites on the surface, n_m, at equilibrium is

$$\frac{n}{n_m} = \frac{KP}{1 + KP} \quad (2)$$

The BET model extends the Langmuir model to multilayers.[10] The energetics of interaction between adsorbing molecules and sites on the surface is described by the constant, K_1, whereas the energetics of interaction between adsorbing molecules that are "stacked" on top of other molecules is described by K_2 (eq 3):

* To whom correspondence should be addressed. E-mail: iaksay@princeton.edu.

(1) Gole, A.; Dash, C.; Mandale, A. B.; Rao, M.; Sastry, M. *Anal. Chem.* **2000**, *72*, 4301–9.

(2) Phadtare, S.; Parekh, P.; Gole, A.; Patil, M.; Pundle, A.; Prabhune, A.; Sastry, M. *Biotechnol. Prog.* **2002**, *18*, 483–8.

(3) Wu, G.; Datar, R. H.; Hansen, K. M.; Thundat, T.; Cote, R. J.; Majumdar, A. *Nat. Biotechnol.* **2001**, *19*, 856–60.

(4) Watson, G.; Staples, E. *Proc. 1990 Ultra-Sonics Symp.* **1990**, *1*, 311–4.

(5) Buttry, D. A.; Ward, M. D. *Chem. Rev.* **1992**, *92*, 1355–79.

(6) Buttry, D. A.; Ward, M. D. *Science* **1990**, *249*, 1000–7.

(7) Datskos, P. G.; Thundat, T. *J. Nanosci. Nanotechnol.* **2002**, *2*, 369–73.

(8) Yi, J. W.; Shih, W. Y.; Shih, W.H. *J. Appl. Phys.* **2002**, *91*, 1680–6.

(9) Li, X. P.; Shih, W. Y.; Vartuli, J. S.; Milius, D. L.; Prud'homme, R. K.; Aksay, I. A.; Shih, W. H. *J. Appl. Phys.* **2002**, *92*, 106–11.

(10) Brunauer, S.; Emmett, P. H.; Teller, E. *J. Am. Chem. Soc.* **1938**, *60*, 309–19.

(11) Gregg, S. J.; Sing, K. S. W. *Adsorption, Surface Area and Porosity*; Academic Press: London, 1982; Chapters 1 and 3.

(12) Emmett, P. H. *J. Am. Chem. Soc.* **1946**, *68*, 1784–9.

(13) Langmuir, I. *J. Am. Chem. Soc.* **1918**, *40*, 1361–1403.

$$\frac{n}{n_\mathrm{m}} = \frac{K_1 P}{(1 - K_2 P)[1 - (K_2 - K_1)P]} \quad (3)$$

The BET model reduces to the model of Langmuir when $P \ll 1$.

The models by Young,[14] Laplace,[15] and later by Kelvin[16] provide the basis for the thermodynamics of liquid-phase condensation at curved surfaces at vapor pressures lower than the vapor pressures at flat surfaces (eq 4):

$$P = P_0 \exp\left[\frac{2\gamma}{n_1 rkT}\right] \quad (4)$$

where P and P_0 are the vapor pressures of a liquid at equilibrium with its vapor across a curved and flat interface, respectively; n_1 is the density of the liquid phase; r is the characteristic radius of curvature; γ is the surface tension of the vapor−liquid interface; k is the Boltzmann constant; and T is the absolute temperature. Because of variations in channel size, capillary condensation occurs over a range of partial pressures. The sharpness of the mass accumulation at a given pressure is a function of the distribution in the characteristic radii of curvature of the surfaces: the narrower the distribution, the sharper the increase and the greater the sensitivity.

Thin Film Coatings. Coatings can be classified as one of four types: monolayers,[17,18] multilayers,[19,20] dense thin films,[21] or porous thin films.[22−29] These coatings introduce specific functional groups that can enhance both the sensitivity and the selectivity of the sensor for particular molecules. Porous thin films, in addition to presenting a specific surface chemistry, also present a finite volume of material (defined by the thickness of the film) that can be accessible to the target molecules.[25,27]

There are three properties of the nanostructures within a porous thin film that affect the sensitivity of the underlying resonator. The first property is the specific surface area per unit mass of the coating, as determined typically by nitrogen sorption measurements.[11] A greater specific surface area results in a larger number of sites for the accumulation of target molecules, and thereby a larger value of $\mathrm{d}m_i/\mathrm{d}P_i$.

The second property is the accessibility of the binding sites to the target molecules. There are two factors that determine accessibility: the characteristic size of the nanostructure (relative to that of the target molecule), and the interconnectedness of the nanostructures. It has been shown that an increase in specific surface area alone may not always lead to an increase in the sensitivity of a resonator to the target molecules.[26,27] Similarly, the role of interconnectedness on accessibility has been demonstrated with a bicontinuous network of pores that run both parallel and orthogonal to the surface of a silica thin film to make the entire volume accessible.[30]

The third property is the uniformity of the nanostructures. Porous materials that are formed by kinetic control typically have large distributions in the characteristic size of the internal structures.[31] An attractive approach to control the uniformity is by templating the matrix of the thin film with surfactant or polymer mesophases to form specific nanostructures[30,32−35] or with colloidal particles to form specific microstructures.[36,37] Removal of the template results in a nano- and/or microstructured material with a uniform characteristic size determined by the template. The relative effect of each of these properties on the sensitivity has not been identified.

To explore the relative importance of the specific surface area, accessibility, and uniformity of the coating to the sensitivity of a resonator to molecules in the gas phase, we use thin films of porous silica with different nanostructures while keeping the surface chemistry fixed (Figure 1). Specifically, we compare the presence of water vapor to the sensitivity of a QCM coated with three different thin films (<1 μm thick) of porous silica: silica xerogel (Figure 1A),[38,39] silica templated with a surfactant-based hexagonal phase (Figure 1B),[40] and silica templated with a surfactant-based disordered L_3 phase (Figure 1C).[38,39] All three silica coatings are expected to have a greater affinity for water molecules than the gold surface of an uncoated resonator. This affinity results from the presence of hydroxyl groups on the silica surface that make favorable hydrogen bonds with water molecules.

The primary structural information of the these silica coatings comes from transmission electron microscopy (TEM)[38−40] and small-angle X-ray scattering (SAXS).[38,39] The silica xerogels (Figure 1A) display a disordered structure produced through the percolation of fractal aggregates: there are no indications of a single uniform channel/pore size.[31,38,39,41−43] Since the wet gel network collapses during drying because of capillary forces associated with the liquid/vapor menisci, the xerogels are much denser than the parent wet gels. In the surfactant-based silica films, the nanostructure is defined by the imprinted space of the surfactant micelles and the membranes that serve as the template for silica condensation to produce the hexagonal phase-templated silica (Figure 1B) and the L_3-templated silica (Figure 1C).[44] Removal of the surfactant is required to make the channels

(14) Young, T. *Philos. Trans. R. Soc. (London)* **1805**, *95*, 65−87.

(15) Laplace, P. S. *Mechanique Celeste*; Chelsea Publishers: New York, 1966; Supplement to Book 10 (original work published 1806).

(16) Thomson, W. T. *Philos. Mag.* **1871**, *42*, 448−52.

(17) Tipple, C. A.; Lavrick, N. V.; Culfa M.; Headrick, J.; Datskos, P.; Sepaniak, N. *J. Anal. Chem.* **2002**, *74*, 3118−26.

(18) Boschkova, K.; Stalgren, J. J. R. *Langmuir* **2002**, 18, 6802−6.

(19) Mermut, O.; Barrett, C. J. *J. Phys. Chem. B* **2003**, *107*, 2525−30.

(20) Khopade, A. J.; Caruso, F. *Langmuir* **2003**, *19*, 6219−25.

(21) Khan, N. A.; Chen, J. G. *J. Vac. Sci. Technol. A* **2003**, *21*, 1302−6.

(22) Mintova, S.; Mo, S. Y.; Bein, T. *Chem. Mater.* **2001**, *13*, 901−5.

(23) Zhao, J.-H.; Malik, I.; Ryan, T.; Ogawa, E. T.; Ho, P. S.; Shih, W.-Y.; McKerrow, A. J.; Taylor, K. *Appl. Phys. Lett.* **1999**, *74*, 944−6.

(24) Krtil, P.; Trojanek, A.; Samec, Z. *J. Phys. Chem. B* **2001**, *105*, 7979−83.

(25) Shinar, R.; Liu, G.; Porter, M. D. *Anal. Chem.* **2000**, *72*, 5981−7.

(26) Bein, T.; Brown, K.; Frye, G. C.; Brinker, J. C. *J. Am. Chem. Soc.* **1989**, *111*, 7640−1.

(27) Yongan, Y.; Bein, T. *J. Am. Chem. Soc.* **1995**, *117*, 9990−4.

(28) Lipert R. J.; Shinar, R.; Vaidya, B.; Pris, A. D.; Porter, M. D.; Lui G.; Grabau T. D.; Dilger J. P. *Anal. Chem.* **2002**, *74*, 6383−91.

(29) Barranco, A.; Cotrino, J.; Yubero, F.; Espinos, J. P.; Gonzalez-Elipe, A. R. *J. Vac. Sci. Technol. A* **2004**, *22*, 1275−84.

(30) Kim, S. S.; Zhang, W.; Pinnavaia, T. J. *Science* **1998**, *282*, 1302−5.

(31) Brinker, C. J.; Scherer, G. W. *Sol−Gel Science*; Academic Press: New York, 1990; Chapters 5 and 9.

(32) Beck, J. S.; Vartuli, J. C.; Roth, W. J.; Leonowicz, M. E.; Kresge, C. T.; Schmitt, C.; Chu, T.-W.; Olson, K. H.; Sheppard, E. W.; McCullen, S. B.; Higgins, J. B.; Schlenker, J. L. *J. Am. Chem. Soc.* **1992**, *114*, 10834−43.

(33) Kresge, C. T.; Leonowicz, M. E.; Roth, W. J.; Vartuli, J. C.; Beck, J. S. *Nature* **1992**, *359*, 710−2.

(34) Monnier, A.; Schuth, F.; Huo, Q.; Dumar, K.; Margolese, K.; Maxwell, R. S.; Stucky, G. D.; Krishnamurthy, M.; Petroff, P.; Firouzi, A.; Janicke, M.; Chmelka, B. F. *Science* **1993**, *261*, 1299−1303.

(35) Hentze, H.-P.; Kramer, E.; Berton, B.; Forster, S.; Antonietti, M. *Macromolecules* **1999**, *32*, 5803−9.

(36) Hall, S. R.; Davis, S. A.; Mann, S. *Langmuir* **2000**, *16*, 1454−6.

(37) Lu, L.; Sun, G.; Xi, S.; Wang, H.; Zhang, H.; Wang, T.; Zhou, X. *Langmuir* **2003**, *16*, 3074−7.

(38) McGrath, K. M.; Dabbs, D. M.; Yao, N.; Aksay, I. A.; Gruner, S. M. *Science* **1997**, *277*, 552−6.

(39) McGrath, K. M.; Dabbs, D. M.; Yao, N.; Edler, K. J.; Aksay, I. A.; Gruner, S. M. *Langmuir* **2000**, *16*, 398−406.

(40) Yao, N.; Ku, A. Y.; Nakagawa, N.; Lee, T.; Saville, D. A.; Aksay, I. A. *Chem. Mater.* **2000**, *12*, 1536−48.

(41) Vollet, D. R.; Donatti, D. A.; Ruiz, A. I. *Phys. Rev. B* **2004**, *69*, 064202.

(42) Schaefer, D. W.; Olivier, B. J.; Ashley, C. S.; Richter, D., Farago, B.; Frick, B.; Hrubesh, L.; Vanbommel, M. J.; Long, G.; Krueger, S. *J. Non-Cryst. Solids* **1992**, *145*, 105−12.

(43) Avnir, D.; Jaroniec, M. *Langmuir* **1989**, *5*, 1431−3.

(44) Dabbs, D. M.; Aksay, I. A. *Annu. Rev. Phys. Chem.* **2000**, *51*, 601−22.
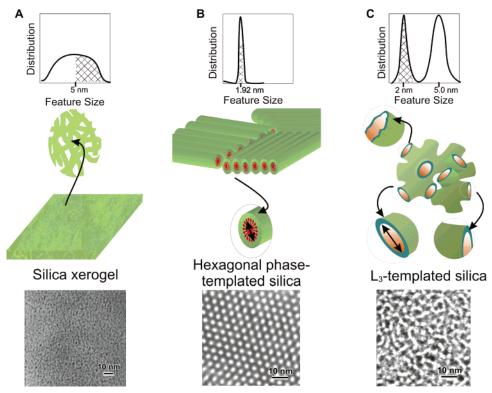
Figure 1. Characteristic size distributions (top), schematics of structures (middle), and TEM images (bottom) of (A) a silica xerogel, (B) hexagonal phase-templated silica, and (C) L_3-templated disordered silica. Shaded regions of the size distributions represent inaccessible regions within the nanostructure. The most prominent feature size is the diameter of the channels (1.92 nm for hexagonal phase-templated silica and 5 nm for the L_3-templated silica). For the L_3-templated silica, the surfactant bilayer has a dimension of 2 nm. The TEM images have been adapted from refs 38 and 44.

accessible in the hexagonal phase-templated silica. The surfactant removal is not necessary to access all the channels in the L_3-templated silica, and the channel size is determined by the composition of the solvent rather than the surfactant length.[38,39] However, if the surfactant is removed, intramembrane space also becomes available. The L_3-templated silica gels display a disordered bicontinuous network of channels that range from 5 to 35 nm, depending on the composition of the surfactant phase.

Experimental Section

Materials. The L_3 template was prepared with cetylpyridinium chloride monohydrate (CpCl), hexanol, NaCl (99%; Aldrich Chemical Co., Inc., Sheboygan Falls, WI), and HCl (aq) (standard 1.0 N solution; Acros Organics, Morris Plains, NJ). These were stored at room temperature and used as received. The 0.2 M chloride solution was prepared by diluting 14% of 0.2 M HCl (aq) (1 part standard 1.0 N solution and 4 parts deionized water; Acros Organics) with 86% 0.2 M NaCl (2.924 g of NaCl in 250 mL of deionized water; Aldrich Chemical Co., Inc.) by volume. Tetramethoxysilane (TMOS; 98%; Aldrich Chemical Co., Inc.) was used as the silica precursor for the synthesis of the L_3-templated silica gel as well as for the synthesis of the silica xerogel.[38,39] The hexagonal phase-templated silica was prepared by mixing cetyltrimethylammonium chloride (CTAC; 25%; Aldrich Chemical Co., Inc.) with tetraethoxysilane (TEOS; Aldrich Chemical Co. Inc.) in an acidic aqueous solvent. Commercial sources of QCMs (5 MHz; Maxtek, Inc., Santa Fe Springs, CA) and polydimethoxysilane (PDMS; Sylgard 184 kit; Dow Corning, Midland, MI) for masking the surface of the quartz crystals were used in all our studies.

Synthesis of Silica Coatings. The L_3 liquid crystal solutions (60 wt % solvent fraction) were made by the procedure outlined previously.[38,39] A mixture of hexanol and CpCl was stirred using a magnetic stir bar to get a uniform paste of the mixture prior to

adding the chloride solvent.[45] Since CpCl, in its as-received form, is in a lamellar structure, this stirring step was essential for conversion to the L_3 structure. The L_3 samples were allowed to equilibrate for 2 days, after which the desired proportions of the silica precursor were added.[38,39]

Hexagonal phase-templated silica was synthesized by using the procedure outlined elsewhere.[40] The molar ratio used for the formation of the films was 4 TEOS/1.2 CTAC/9.2 HCl/1000 H_2O. The reagents were mixed vigorously until TEOS was dissolved, as indicated by the formation of a clear solution.

For the synthesis of silica xerogel, TMOS was added to a 0.2 M chloride solvent such that the water-to-alkoxide molar ratio was maintained at 4:1. This ratio was chosen to be consistent with the proportions of the solvent and silica precursor used during the synthesis of the L_3-templated silica gel.

Formation of Silica Coatings. Both sides of quartz disks were first coated with 6 nm of chromium followed by 60 nm of gold electrode coating. Solutions of 60 wt % L_3-templated silica, silica xerogels, and hexagonal phase-templated silica were then used to form thin films on the gold electrodes. Quartz crystals were prepared for dip coating by cleaning the surface with piranha solution (70% sulfuric acid (95−98%) plus 30% hydrogen peroxide (30%, aq), by volume; Aldrich Chemical Co., Inc.) for 5−10 min, followed by rinsing with deionized water.

The L_3-templated silica and silica xerogel films were prepared via dip coating at a speed of 6 cm/min. A PDMS mask was used to cover the lower side of the quartz crystal while coating the upper electrode of the QCM. The dimensions of the mask were similar to that of the crystal (diameter 2.54 cm). The PDMS mask prevented contact between the silica gel and the lower electrode of the crystal. Silica solutions of desired concentration were used for dip coating 30 min after the silica precursor was added to the liquid crystal solution. This time allowed the initiation of the hydrolysis−

(45) Bhansali, S.; Malik, S.; Jarvis, J. M.; Akartuna, I.; Dabbs, D. M.; Carbeck, J. D.; Aksay, I. A. *Langmuir* **2006**, *22*, 4060−4.

condensation reaction between the silica precursor and the solvent before coating. The crystals coated with the L_3-templated silica were stored in 2-propanol overnight to assist in the gel formation and to prevent shrinkage of the silica network. These silica films were dried in a 60 °C oven to eliminate organic volatiles from the silica matrix. The crystals coated with silica xerogel were thermally treated in air at 300 °C.

The hexagonal phase-templated silica films were prepared by growing films on the upper electrode of the crystal. The upper surface of the crystal was aligned with the air−liquid interface of the solution in a Petri dish. The crystal was supported by two PDMS spacers between the crystal and the bottom of the dish. The crystals were collected after 2 h and stored in the supernatant solution for several days. Crystals coated with the ordered silica films were air-dried and calcined at 400 °C.[40] The heat-treated films were stored in a vacuum oven prior to use to prevent moisture from adsorbing onto the films.

Small-Angle X-ray Scattering. One-dimensional SAXS data on hexagonal phase-templated silica particles were collected using a compact Kratky camera (Anton-Paar, Graz, Austria) connected to a position-sensitive detector. (Braun OED-50M, MBraun, Graching, Germany). The raw data were reduced using previously reported procedures.[46] Cu K_α radiation was used in all X-ray analysis.

Water Vapor Accumulation Experiments. An impedance/gain phase analyzer (4194A impedance analyzer, Hewlett-Packard Co., Palo Alto, CA) was used to measure the impedance and phase angle responses of both the coated and uncoated quartz disks as a function of frequency. All disks had an approximately 5 MHz resonance frequency and a thickness of 186 μm. The quartz disks were placed in a quartz crystal holder (Maxtek, Inc.; the quartz crystals were placed in a CHC-100 crystal holder) connected to a test fixture (16047 D test fixture, Hewlett-Packard Co.) attached to the analyzer. Before any measurements were made, the crystal surface was purged with N_2 until a stable frequency baseline was obtained.

The water vapor accumulation was measured on both the uncoated and the coated disks by increasing the relative humidity in the chamber holding the quartz crystal. This was done by altering the concentrations (flow rate) of air and nitrogen flowing into the chamber. Air was passed from a laboratory airline to a 500 mL flask containing water. The flask was placed on a hot plate. The heated air was directed into a 7.6 L Nalgene container that enclosed the QCM setup. A hygrometer (traceable hygrometer/thermometer with memory and probe, VWR International, Bridgeport, NJ) was used to monitor both the relative humidity and temperature inside the chamber. In all data collection, the system was allowed to equilibrate for 5−10 min to allow for transport of the vapor across the silica film.

Results and Discussion

In the absence of any coating, the resonant frequency of a QCM decreased by 25 Hz with the accumulation of water vapor up to a relative partial pressure, P/P_0, of 1. The resonant frequency shifted further with the silica-coated QCMs. Using the Sauerbrey relationship,[47] we related the shift in resonant frequency to a change in the mass of the resonator. Figure 2 shows the accumulation isotherms of water on coated resonators as a function of the partial pressure of the water. [The mass of the silica films was determined by subtracting the resonance frequency of the coated QCM (f_1) from the resonance frequency of the uncoated QCM (f_0). The mass of accumulated water vapor at a partial pressure P/P_0 was determined by subtracting the resonance frequency at the partial pressure P/P_0 (f_2) from the resonance frequency of the coated QCM (f_1).] The differences in the role of the coatings on mass accumulation are striking. Below, we relate these differences to the variations in the nanostructure of the coatings.
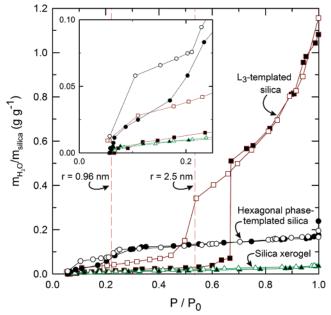
(46) Register, R. A.; Bell, T. R. *J. Polym. Sci., Part B: Polym. Phys.* **1992**, *30*, 569−75.

(47) Sauerbrey, G. *Z. Phys.* **1959**, *155*, 206−22.

Figure 2. Mass sensitivity for QCMs modified with three different films. Green triangles, black circles, and red squares represent the accumulation isotherms for the silica xerogel, the hexagonal phase-templated silica, and the L_3-templated silica films, respectively. The open symbols represent the isotherm generated by decreasing the partial pressure of water vapor. The inset shows the isotherm for partial pressures less than 0.25. The red dashed lines indicate the regions of capillary condensation for the hexagonal phase-templated silica ($P/P_0 = 0.26$) and L_3-templated silica ($P/P_0 = 0.54$). The radii of curvature as determined by the Kelvin equation (eq 4) at $P/P_0 = 0.26$ and 0.54 are indicated.

The Role of Coatings on Accumulation. At low pressures ($P/P_0 < 0.2$), the mass accumulation for all three films increases monotonically but with different amounts, whereas, at higher pressures, both surfactant-templated films display sudden increases in accumulation. The monotonic increase at $P/P_0 < 0.2$ is consistent with monolayer adsorption, as described by the Langmuir model.[13] At $P/P_0 > 0.2$, the accumulation in xerogel films does not saturate but rather continues to increase, albeit at a rate lower than that observed for values of $P/P_0 < 0.2$, reaching a maximum of ∼0.03 g of water per gram of silica as $P/P_0 \rightarrow 1$. This behavior is consistent with multilayer adsorption, as described by the BET model. The absence of any large increase in accumulation with increasing P indicates that $(K_2 - K_1)P$ never reaches a value of 1, even as $P/P_0 \rightarrow 1$.

The hexagonal phase-templated silica films also exhibit an accumulation behavior similar to that observed for the silica xerogel films at $P/P_0 < 0.2$ but with a greater accumulation. As detailed below, we attribute this greater accumulation to a higher surface area of the hexagonal phase-templated films available for adsorption. At $P/P_0 \approx 0.2$, the isotherm for the hexagonal phase-templated silica film displays a sudden increase in the mass accumulation. One interpretation of this increase is that the quantity $(K_2 - K_1)P$ approaches a value of 1 at this partial pressure. However, this seems unlikely since the values of K_1 and K_2 should not differ between the silica xerogel and the hexagonal phase-templated silica.

An alternative explanation for this sudden increase in mass accumulation is the liquid-phase condensation within the nanostructure of the hexagonal phase-templated silica film, as predicted by the Kelvin model.[16] For values of $P/P_0 > 0.4$, the change in mass accumulation with increasing partial pressure is again similar to that observed with the silica xerogel film. The maximum accumulation of 0.24 g of water per gram of the silica

Table 1. Specific Surface Areas for the Three Materials Used as Well as the Mass Loading at 0.2 and 0.7 Partial Pressures of Water Vapor

coatings	specific surface area $(m^2 \, g^{-1})^a$	radius of curvature from Kelvin model $(nm)^b$	mass of water vapor per unit mass of silica film $(g \, g^{-1})^c$ at $P/P_0 = 0.2^c$	mass of water vapor per unit mass of silica film $(g \, g^{-1})$ at $P/P_0 = 0.7^c$
silica xerogel	78	NA	0.009	0.025
hexagonal phase-templated silica	792	0.96	0.064	0.146
L$_3$-templated silica	282	2.5	0.024	0.473

^{a} Specific surface areas determined using the BET equation (eq 5) on the water vapor accumulation isotherms. ^{b} Diameter determined using the Kelvin equation (eq 4). ^{c} Mass of water vapor accumulation calculated as an average of the values collected while increasing and decreasing relative pressure of water vapor.

film is, however, nearly an order of magnitude greater than that observed with the silica xerogel film. Also, unlike the accumulation isotherm for the silica xerogel film, the isotherm for the hexagonal phase-templated silica shows hysteresis. The isotherm generated by decreasing the partial pressure of water vapor indicates that, even at the lowest partial pressure (0.052 P/P_0), a small quantity of water (0.012 g g^{-1}) is retained within the film unless the film is heat treated at elevated temperatures (inset of Figure 2).

The isotherm for the L$_3$-templated silica film shows a monotonic increase up to partial pressures of 0.66, suggesting monolayer or multilayer adsorption in this region.[10-12] At $P/P_0 \approx 0.66$, a large and sudden increase in mass accumulation to 0.5 g of water per gram of silica film is observed. As P increases beyond this point, the accumulation of water continues to increase up to a maximum of 1.2 g of water per gram of silica. We again interpret this sudden increase as an indication of capillary condensation of liquid water within the nanostructures of the film. Hysteresis is also observed in the L$_3$-templated silica films, however, with a much larger shift than that observed in the hexagonal phase-templated silica films. Similar to the hexagonal phase-templated silica films, a small quantity of water vapor (0.009 g g^{-1}) is retained in the film, which is removed by heat treatment (inset of Figure 2).

There have been several studies to explain the accumulation hysteresis observed in isotherms of interconnected porous networks similar to the structure of the L$_3$-templated silica.[11,48-50] One explanation for hysteresis is the differences between the advancing and receding contact angles of the liquid with the solid. Another explanation is that condensation requires a degree of supersaturation for the nucleation of the condensed phase, and thus the pressures at the onset of condensation are higher than the thermodynamic equilibrium values.[49,50] Hysteresis has also been shown to be a function of the geometry of the underlying porous structure. As the condensed phase vaporizes during pressure decrease, its release from the porous structure can be obstructed if the adjacent channels are still filled with the liquid phase. Thus, liquid-filled pores can block the vaporization from adjacent pores, resulting in the observed hysteresis.[49] We attribute the less pronounced nature of hysteresis in the hexagonal phase-templated silica to its oriented cylindrical channel structure versus the disordered structure of the L$_3$-templated silica.

For the region of the isotherms of low partial pressure, where adsorption dominates the accumulation of water vapor, we apply the BET model to determine the specific surface area of the silica films.[10-12] The BET model (eq 3) can be expressed in an alternative format (eq 5):

$$\frac{x}{n(1-x)} = \frac{1}{n_m c} + \frac{c-1}{c}x \qquad (5)$$

where n_m is the monolayer capacity, $x = P/P_0$, and c is a constant function of K_1 and K_2 and is independent of x. The slope and the intercept of a plot of $x/(n(1-x))$ versus x are used to calculate the monolayer capacity (n_m) of the adsorbent, which is used to determine the specific area, $S_{BET} = a n_m L$, where a is the cross-sectional area of the adsorbate molecule, and L is Avogadro's number.[12] Because the three films have the same surface chemistry, analysis using the BET model should provide an accurate comparison[51] of the *relative* specific surface areas of the three coatings.

At larger values of P/P_0, the accumulation isotherms of the hexagonal phase-templated and L$_3$-templated silica indicate capillary condensation. Then, by using the Kelvin model for the isotherm generated by decreasing the partial pressure of water vapor,[11,52] we determine a characteristic radius of curvature of the nanostructures of the films as 0.96 nm for the hexagonal phase-templated silica and 2.5 nm for the L$_3$-templated silica, as indicated by the vertical dashed lines in Figure 2. In contrast, the silica xerogel does not have a single well-defined radius of curvature, and thus it does not display a noticeable capillary condensation behavior. It is also possible that the water at low relative partial pressure fills the smaller structures and thereby leaves the larger structures inaccessible for condensation.[31]

Table 1 summarizes the structural properties of the three silica coatings as determined from the BET and Kelvin models. To indicate the effect of the structural features on the sensitivity of the resonator, we also list the mass of water vapor accumulated at two values of relative partial pressure, 0.2 and 0.7.

The Effect of Specific Surface Area. At low relative partial pressure ($P/P_0 = 0.2$) data presented in Table 1 show that the amount of water vapor accumulation correlates with the specific surface area: the larger the specific surface area, the greater the mass of water accumulated. The surface area of the hexagonal phase-templated silica film is almost 3 times greater than that of the L$_3$-templated silica film and an order of magnitude greater than that of the xerogel film. The difference with respect to the L$_3$-templated silica film can be attributed to the differences in the temperatures at which the two films were thermally treated. The L$_3$-templated silica films were only annealed at 60 °C, whereas the hexagonal phase-templated silica films were heat treated at 400 °C to remove the embedded surfactant. If we assume that the structure of the silica walls for both of the surfactant-templated films is similar to that of sol−gel processed silica, the differences in the surface areas of these films can be explained with the aid of the study done by Brinker et al. who

(48) Nicholson, D.; Petropoulos, J. H. *J. Phys. D: Appl Phys.* **1968**, *1*, 1379−85.

(49) Liu, H.; Zhang, L.; Seaton, N. A. *Langmuir* **1993**, *9*, 2576−82.

(50) Foster, A. G. *Trans. Faraday. Soc.* **1932**, *28*, 645.

(51) Harris, B. L.; Emmett, P. H. *J. Phys. Chem.* **1949**, *53*, 811−25.

(52) Sing, K. S. W.; Williams, R. T. *Adsorpt. Sci. Technol.* **2004**, *22*, 773−82.

showed the surface area for silica xerogels to be a function of the processing temperature.[53] For temperatures up to 275 °C, the skeletal density of the gel decreases as a result of desorption of physically adsorbed solvents, resulting in an increased surface area.[53] Beyond 275 °C, the skeletal density of the silica increases while the surface area decreases. However, at 400 °C, the surface area is still higher ($\sim$100 m^2/g) than the specific area for processing temperatures of 200 °C. Hence, it is expected that the surface area of silica processed at 400 °C would be substantially higher than that processed at 60 °C.

We attribute the higher surface area differences between the templated silica films and that of the xerogel film primarily to the presence of additional surface area generated by templation. The silica wall densities may also contribute to this difference. For instance, since the hexagonal phase-templated silica films were annealed in supernatant solution prior to thermal treatment, the relatively condensed silica network within the walls will not fold and crumple as much during the drying process. As a result, the hexagonal phase-templated silica films have surface areas that are significantly higher than those of the silica xerogel films.

At a larger value of relative partial pressure ($P/P_0 = 0.7$), however, a larger surface area does not necessarily correlate with increased mass accumulation. This point is clearly illustrated by comparing the mass of water accumulated at a relative partial pressure of 0.7 by the two silica films templated with either the hexagonal or L$_3$ mesophases. Although the specific surface area of the hexagonal phase-templated silica film is nearly 3 times greater than that for the L$_3$-templated silica film, the L$_3$-templated silica film accumulates water per unit mass of the film 3 times that for the hexagonal phase-templated silica film. These differences most likely reflect the accessibility of the nano-structures within the films.

The Effect of Accessibility. We interpret the differences in the maximum water accumulation of the L$_3$-templated silica, in comparison with the silica xerogel and the hexagonal phase-templated silica films in terms of the relative accessibility of the pores. The silica xerogel is known to contain nonuniform channels. The channel sizes can be as small as 1 nm and as large as 10 nm; the size distribution depends on the synthesis conditions.[31] Accumulation of water in the smallest channels near the surface of the film may limit the accessibility to larger channels within the film.[31] The main difference between the L$_3$-templated silica and the hexagonal phase-templated silica relates to the fact that, while the L$_3$ phase is bicontinuous, the hexagonal phase is not. Further, the hexagonal phase-templated silica is not a single crystal. Figure 3 shows the SAXS pattern of the hexagonal phase-templated silica particles precipitated from the supernatant solutions. The presence of two distinct peaks, which correspond to spacings of 1 and $\sqrt{3}$, indicates randomly oriented domains of hexagonally packed cylinders with an average center-to-center distance of 4.1 nm. The inset in Figure 3 shows a magnified view of the second peak. The broadness in the peaks is attributed to the disordered structure at the domain boundaries within these films, identified previously.[40] We expect that there are grain boundaries between crystallites that inhibit the transport of water vapor throughout the film. The channels in these films are also oriented preferentially in a direction parallel to the film surface; this orientation may also restrict the transport of vapor across the entire film. Disordered domains present at the grain boundaries could alleviate some of these limitations to accessibility.[40] In contrast, the large accumulation of mass of water in the L$_3$-templated silica films reflects the disordered structure of the
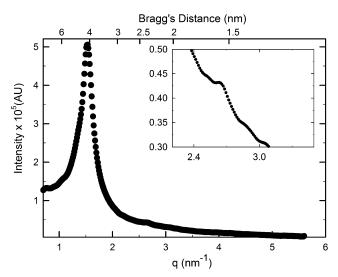

Figure 3. SAXS pattern from hexagonal phase-templated silica particles.

channel network, which allows the channels to be accessed across the entire thickness of the film.[38,39]

The Effect of Channel Uniformity. The partial pressure at which capillary condensation occurs is determined by the characteristic radii of curvature of surfaces that make up the nanostructure.[16] For a material with uniform channels, condensation as a result of this depression in the equilibrium partial pressure occurs over a narrow range of partial pressure, and thereby results in a sharp increase in the mass of accumulated water. The sharpness of the increase, which is a direct measure of the sensitivity as defined by eq 1, is therefore a function of the distribution in size of nanostructures within the film.

The characteristic radius of the channels in the templated silica films determined from the mass accumulation of water can be compared to the characteristic dimensions determined by SAXS. The SAXS pattern of the hexagonal phase-templated silica (Figure 3) shows a characteristic distance of 4.1 nm, which includes the thickness of the walls of the silica enclosing the channel. TEM images reveal a wall thickness of $\sim$1 nm, indicating that the channel should have a diameter of $\sim$2.1 nm compared to 1.92 nm given by the Kelvin analysis.[16]

SAXS on bulk samples of L$_3$ silica revealed a characteristic spacing of 16 nm for a 60 wt % solvent concentration,[38] which is significantly larger than the radius of curvature (2.5 nm) estimated by the Kelvin model. The difference is due to the fact that capillary condensation and X-ray scattering measure different properties of a porous material. X-ray scattering measures length scales over which there is significant variation in the electron density of the material. Capillary condensation measures the presence of curved surfaces that support the condensation of liquid with an air−liquid interface of a characteristic radius of curvature. This radius is interpreted to be representative of the radius of curvature of the underlying surface. The distances probed by SAXS include that of the bilayer of the surfactant as well as the thickness of the silica walls and is therefore expected to be larger than the radius of curvature estimated by the Kelvin model.[38]

Sensitivity Enhancement. We compared the sensitivity, given by eq 1, of an uncoated quartz resonator with resonators coated with the three silica films in the entire pressure range (Figure 4). An uncoated resonator shows a maximum increase in mass per unit increase in the partial pressure of water vapor (dm/d$P_i)_{P/P_0}$ = 1 of 0.42 μg per unit of partial pressure (inset of Figure 4). For partial pressures $P/P_0 <$ 0.4, the hexagonal phase-templated silica films demonstrate the greatest sensitivity to water
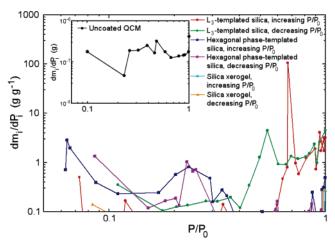
(53) Brinker, C. J.; Roth, E. P.; Scherer, G. W.; Tallant, D. R. *J. Non-Cryst. Solids* **1985**, *71*, 171−85.

Figure 4. The sensitivity of the coated QCMs (dm/dP_i) as a function of the partial pressure of water vapor. The inset shows the data for uncoated QCMs.

detection. The higher sensitivity of the hexagonal phase-templated silica up to $P/P_0 = 0.2$ is by virtue of its larger specific area, and, for the range $0.2 < P/P_0 < 0.4$, it is due to capillary condensation within the nanostructures. On the other hand, for partial pressures $P/P_0 > 0.4$, the sensitivity of the L_3-templated silica film is the greatest of the three films because of a higher amount of accumulation by capillary condensation. All three coated resonators showed enhanced sensitivity to water vapor relative to the uncoated resonator: for partial pressures between $0.05 < P/P_0 < 0.4$, the hexagonal phase-templated silica films show an increase in sensitivity anywhere between 3 and 700-fold; for $0.4 < P/P_0 < 1$, the L_3-templated silica films show an increased sensitivity anywhere between 2 and 4000-fold. The silica xerogel films show an enhanced sensitivity between 1 and 20-fold greater than the uncoated resonator for $0.05 < P/P_0 < 1$.

Conclusions

We have shown the role a continuous film of a nanoporous material can play in the enhancement of the sensitivity of resonators to the presence of specific target molecules in the gas phase. We have demonstrated that a combination of the specific surface area, accessibility, and uniformity of the characteristic radii of curvature of the nanostructure within the porous film determines the mass accumulation of target molecules over a large range of partial pressures. We have shown this by comparing the mass accumulation of water vapor in three silica coatings with different nanostructures: silica xerogel with a disordered structure, silica templated by an ordered hexagonal phase, and silica templated with a disordered, bicontinuous L_3 structure. Increasing specific surface area enhances mass accumulation at low partial pressures ($P/P_0 < 0.2$), whereas uniformity and accessibility of the nanostructures play the dominate role in determining mass accumulation at greater partial pressures ($P/P_0 > 0.2$). Use of both the specific surface area and uniformity of the nanostructure to enhance resonator sensitivity is only possible provided the nanostructures within the films are accessible to the target molecules. We anticipate that if L_3-templated silica films were to be heat treated at higher temperatures to remove the surfactant component and thus create larger specific surface areas, the sensitivity of these films in the low partial pressure regions ($P/P_0 < 0.4$) will be higher.[54,55] The unique nanostructure of the L_3-templated silica coating provides this accessibility and thereby demonstrates increased resonator sensitivity relative to the other coatings. This approach, however, is not limited to the detection of water vapor; it should be directly applicable to the sensing of other gases. Some of the ideas presented can also be extended to improve the performance of sensors used in liquid environments.

(54) Dabbs, D. M.; Mulders, N.; Aksay, I. A. *J. Nanopart. Res.*, in press.
(55) Malik, A.-S.; Dabbs, D. M.; Katz, H. E.; Aksay, I. A. *Langmuir* **2006**, *22*, 325−31.